Physics studies of the improved H-mode scenario in ASDEX Upgrade

J. Stober[1], A.C.C. Sips[1], C. Angioni[1], C. Forest[2], O. Gruber[1], J. Hobirk[1], L.D. Horton[1], C.F. Maggi[1], M. Maraschek[1], P. Martin[3], P. McCarthy[4], V. Mertens[1], Y.-S. Na[5], M. Reich[1], A. Stäbler[1], G. Tardini[1], H. Zohm[1], and the ASDEX Upgrade Team

[1] Max-Planck-Institut für Plasmaphysik, EURATOM-Association, Garching, Germany
[2] Dept. of Physics, University of Wisconsin, Madison, USA
[3] Consorzio RFX, Associazione Euratom-ENEA sulla Fusione, Corso Stati Uniti 4, I-35127 Padova, Italy
[4] Dept. of Physics, University College Cork, Assosiation EURATOM-DCU, Cork, Ireland
[5] National Fusion Research Center, 52 Yeoeun-Dong, Yusung-Gu, Daejeon, 305-333, Korea
e-mail: Joerg.Stober@ipp.mpg.de

Abstract
Recent studies at ASDEX Upgrade aim to further characterise and understand the physics of the improved H-mode. The main focus is on the influence of the ramp-up scenario for plasma current and heating on energy confinement and MHD-activity during the subsequent steady state phase. Depending on the ramp-up scenario two different stationary plasmas can be generated, which show different equilibrated current profiles. The difference of the current profiles seems to be due to different MHD modes, which set in during the current profile evolution. Also the stored energy is different in the two cases as well as the peaking of the temperature profiles. This may be due either to increased transport by MHD modes themselves or to the variation of the ratio of magnetic shear s to safety factor q, which modifies the critical temperature gradient-length for the onset of ITGs. These core profile variations make up for part of the difference of the stored energy, but also the pedestal pressures are remarkably different as analysed on the basis of high-resolution Thomson-Scattering measurements at the plasma edge.

1. Introduction

The 'improved H-mode' regime of ASDEX Upgrade [1], a candidate for the ITER hybrid scenario, has been confirmed on several other devices [2–4]. Hybrid operation in ITER aims at reduced plasma current to extend the duration of the plasma, but maintaining dominant α-particle heating ($Q = 10$). Alternatively, at full plasma current, the base line performance of ITER could be significantly exceeded if improved H-mode parameters can be achieved [5]. However, significant debate remains on which ingredients are essential for improved H-mode operation and what the differences are compared to 'standard' H-modes. Moderate additional heating during the plasma current ramp-up is thought to be a key ingredient to form an adequate current profile for stronger heating in the flat-top phase. This stronger heating phase itself usually starts with a power level well above the threshold for type-I ELMy H-mode aiming at a value of $2.0 < \beta_N < 2.5$, and is then kept for a significant part of a current diffusion time before the power is ramped up further to obtain the highest β_N-value, limited by the onset of (2,1)-NTMs for $\beta_N \approx 3$. The latter high-β phase is envisaged for the ITER hybrid scenario. The phase with constant intermediate power turns out to be important to prevent an early onset of strong NTMs in the final high power phase. The phenomenological dependence of the plasma state on time scales in the order of the current diffusion time indicates that the current profile is an important ingredient in the process. So far, the underlying physics is not really understood. A central element in the discussion is the suppression of sawteeth allowing higher beta-values by elimination of seed-islands for detrimental NTMs. Still small NTMs as well as small sawteeth are found in some of the high-β phase without detrimental effects. Results from DIII-D [2] show an inverse relation between the size of an (3,2)-NTM and the size of the sawteeth, indicating that a small (3,2)-NTM can indeed limit the sawteeth size making it less effective as a seed for an (2,1)-NTM or even eliminates the sawteeth. These findings indicate that the central q-profile

is modified in presence of NTMs. Still there are open questions on why the NTM is created and why it stays small and how this relates to the heating in the ramp-up phase. Another observation still lacking explanation is the small power degradation of the energy confinement time with increasing heating power, such that the high β-values are achieved with H-factors well above unity (referring to the ITER reference scaling IPB-H98(y,2)) [6]. Here core and pedestal effects still have to be separated.
There are several contributions to this conference reporting studies at ASDEX Upgrade on the improved H-mode/ITER-hybrid-scenario: The performance of the strong heating phase (hybrid-phase) over a wide operational range, its dependence on machine conditions, and its extrapolation to ITER is described in [7]. The high resolution pedestal measurements and details of the pedestal evolution with increasing heating power are described in [8]. These are compared to the findings of other machines on the pedestal behaviour in improved confinement discharges in [9]. The contribution in hand mainly addresses physics issues in the first two phases of the improved H-mode scenario. The influence of heating and gas puffing during the phase of current ramp-up on the current profile as well as MHD and core transport in the subsequent phase with $2.0 < \beta_N < 2.8$ are studied systematically. An early-heating and a late-heating scheme are compared in detail with respect to core and edge profiles.

2. Variation of the ramp-up scenario

The current ramp-up phase is thought to be crucial for improved H-mode operation in the sense of sawtooth prevention. Early additional heating in the current ramp-up increases the electron temperature and therefore the current diffusion time, such that the loop voltage applied by the central solenoid penetrates less towards the plasma centre and the resulting plasma-current profile at the start of the flat-top phase is less peaked or even hollow keeping the central safety factor well above unity. On the other hand, too much power in the preheat is known to generate short-lived ion-ITBs in the subsequent main heating phase. Still the optimum shape of the q-profile is not obvious and usually it is determined in a trial and error procedure, such that the ramp-up scenario varies between machines. In ASDEX Upgrade the ramp-up scheme had to be changed when the inner heat shield was coated with tungsten in 2003. Before, this heat shield was used as high-field-side limiter during the whole ramp-up phase. Afterwards, the change-over to a diverted shape was timed as early as the NBI is switched on. The usual criterion to accept a ramp-up scenario as reasonably optimised is that a type-I ELMy H-mode with no or modest sawteeth evolves and that high β-values are obtained in the high-power hybrid-phase. It was therefore surprising to observe in ASDEX Upgrade that an explicit late heating scheme with a long ohmic phase before adding auxiliary heating resulted in a better performance (higher W_{mhd} and H-factor) as compared to the dedicated early heating scheme. The corresponding time traces are shown in figure 1. This result obviously questions the above mentioned ideas on the effect of the current ramp-up phase.

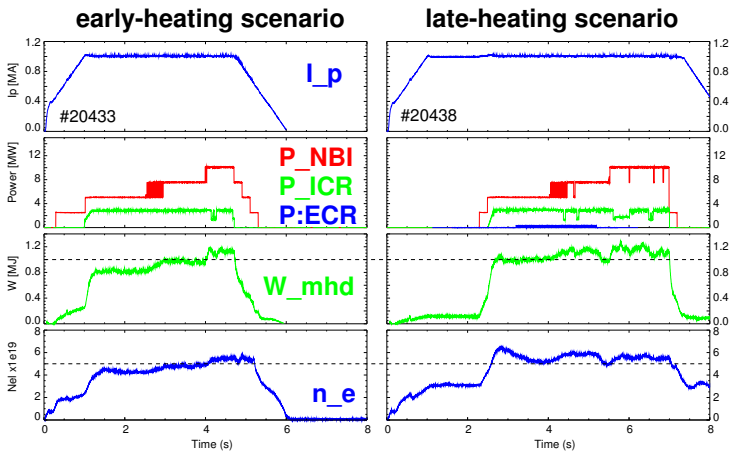

Figure 1: Effect of ramp-up scenario on improved H-mode performance at different power levels.

Therefore a systematic study of the early heating phase was performed varying heating power and gas puff at two different values of the toroidal field (2.0 T and 2.4 T, corresponding to q_{95} values of 4.0 and 4.8). The results were compared to the late heating scheme, also at both values of q_{95}. The main heating phase was kept at a constant level of 8 MW for all discharges including 3 MW of central ICRH to prevent central accumulation of heavy impurities. This occurs with pure NBI-heating in this scenario since large parts of the first wall of ASDEX Upgrade have been covered with tungsten [7]. Since stray radiation from the ICRH-plant is suspected to disturb the MSE measurement ICRH is switched off 50 ms out of 500 ms and is substituted by another NBI source. The choice of NBI sources was the same in all discharges, such that profiles of the NBI driven current and momentum input are similar. Co-injecting NBI sources are used: one beam, which is also used in the current ramp-up, passes through the plasma center, whereas another one is off-axis [10]. A third beam similar to the first one is used to substitute the ICRH during the short intervals for MSE measurements. Due to the variation of τ_E and B_t, β_N ranges from 2.0 to 2.8 in these discharges. It was deliberately chosen not to increase the heating power to the β-limit towards the end of the discharge, but to let the current profile completely evolve. The objective was to check whether the current profiles which we observe in the main heating phase are really separate (meta)-stable states or if they evolve towards a common equilibrium with similar MHD-modes. Figure 2 illustrates the two ramp-up schemes by time traces for an early-heated and a late-heated discharge at $q_{95} = 4.8$. Figure 3 shows the variation of the q-profiles which has been achieved at the onset of the main heating by the variation of the start-up scenario. All discharges have otherwise identical control parameters, i.e. 1.0 MA plasma current, same shape, no additional fuelling during the

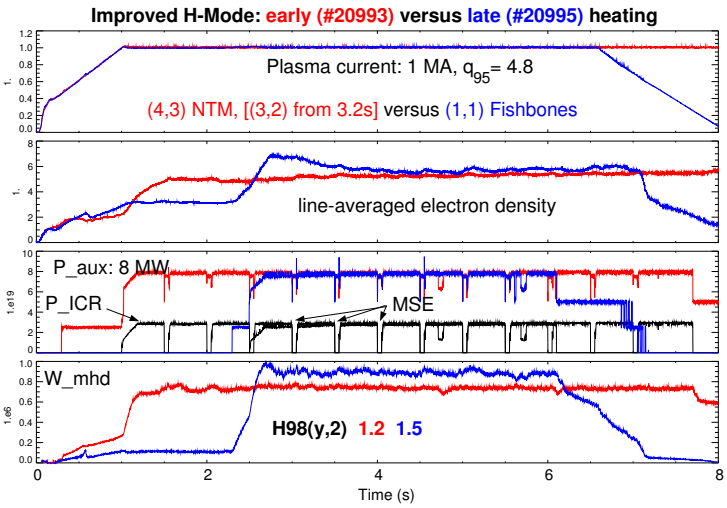

Figure 2: Time traces for study on current ramp up.

#	Te0 (1.0 s)	$\langle ne \rangle$ (1.0 s)	PNBI (preheat)	q0	q95	$H98_{y,2}$	MHD behaviour during high power phase
	[keV]	1E19m^{-3}	[MW]				
20998	3.0	2.5	2.5	2.0	4.0	-	Disrupts after ITB
20993	3.4	2.2	2.5	3.2	4.8	1.2	4/3 NTM, 3/2 NTM at 3.2s
20991	2.6	3.6	2.5	2.8	4.8	1.2	4/3 NTM, 3/2 NTM at 2.3s
20990	2.2	5.5	2.5	2.2	4.8	1.2	4/3 NTM, 3/2 NTM at 1.8s
20992	1.5	5.3	1.25	?	4.8	1.2	4/3 NTM throughout
20994	1.6	2.9	0	1.0	4.8	-	Fishbones, wall contact
20995	1.6	2.9	0	0.95	4.8	1.5	Fishbones throughout
20996	1.1	2.9	0	0.8	4.0	1.5	Fishbones
20997	1.1	2.9	0	0.8	4.0	1.5	4/3 NTM $\rightarrow$ Fishbones
20999	1.0	5.2	1.25	?	4.0	1.2	4/3 NTM throughout

Table 1: Parameters of current ramp-up study. All discharges have some sawteeth, partly synchronised with ICRH modulation. q_0 is given at the onset of the main heating, i.e. at 1.0 s with preheat and at 2.5 s without. A level of 1.25 MW of preheat is achieved by on-off modulation of the 2.5 MW beam used for MSE, such that no reasonable measurement is possible. This is indicated by a '?' in the 'q0' column. The H-factor refers to the steady-state phase at 5.5 s in all cases.

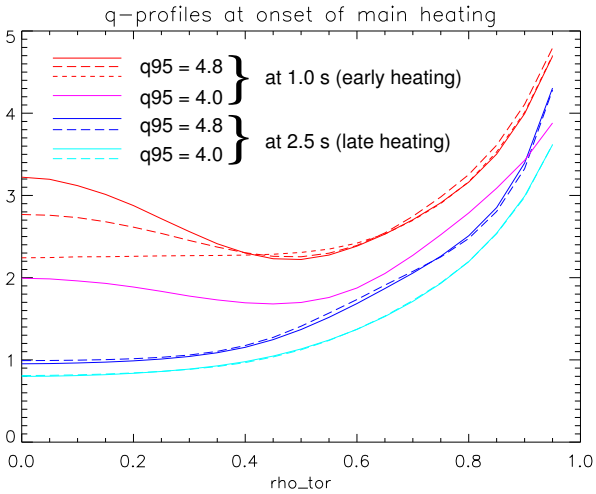

Figure 3: Variation of q-profiles at the onset of the main heating obtained by modification of the ramp-up phase. Red: early heating q_{95}=4.8 varying gas puff, magenta: early heating q_{95}=4.0, blue: late heating q_{95}=4.8, cyan: late heating q_{95}=4.0. For the latter two, dashed lines refer to repeated discharges.

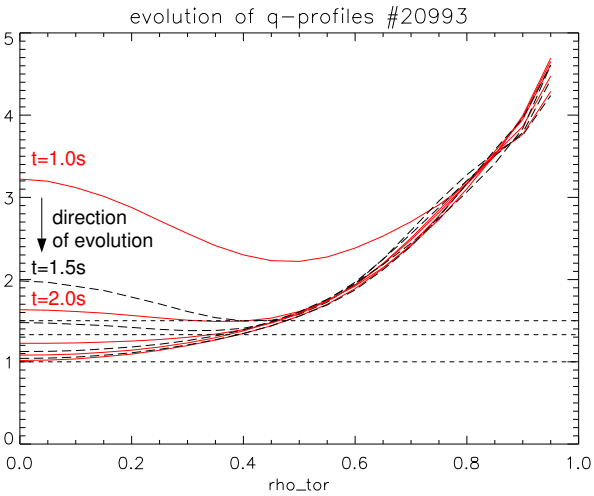

Figure 4: Evolution of the q-profile during the main heating phase for the most inverted q-profile in figure 3 (early-heating case in figure 2). Evolution is shown in 0.5s steps starting at 1.0 s. Central q_0 evolves towards lower values. The three horizontal lines indicate resonant q-values.

main heating phase. Table 1 lists the modifications during current ramp-up, the achieved values for q_0 at the onset and H-factors and MHD-modes towards the end of the main heating. The evolution of the current profile during the main heating phase is shown in figure 4 for the discharge with the most strongly inverted q-profile at the onset of the main heating. The major changes are observed for the first half second but a steady state is only reached after 3 seconds of flat top. During this evolution of the current profile, a (4,3)-NTM occurs at 2 seconds followed by the occurence of a (3,2)-NTM at 3.2 seconds. Figure 5 shows that the equilibrated q-profiles are only marginally different for all q_{95}=4.8 case with early heating, essentially independent from the variations of heating power and gas puff in the preheat phase. The case with strongest gas puff (#20990) shows small sawteeth, but no difference with respect to confinement or other MHD activity is observed. Comparing the blue curves in figures 3 and 5 we note, that the current profile obtained with the late-heating scheme remains almost unchanged, i.e. it is already close to its equilibrated shape. The first discharge at lower q_{95} showed a strong sensitivity to the periodic switching of ICRH and NBI, such that this switching has been excluded for the other discharges at this q-value, such that no MSE values are available. As shown in table 1, for q_{95}=4.0 the early heating scenario with the highest level of early heating did not yield a

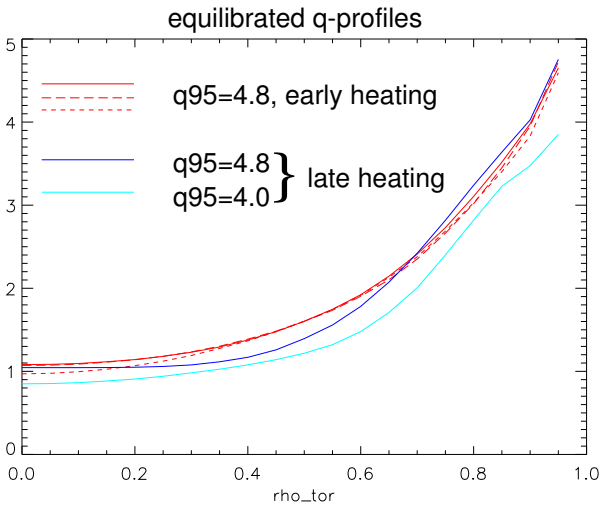

Figure 5: Equilibrated current profiles (at 5.5 s), same linestyle/colour-code as in fig. 3. (if MSE is available). Errors are discussed in the text on the basis of figure 6. Only the short dashed red case (#20990, see table 1) shows regular sawteeth not related to ICRH modulation.

steady state H-mode during the main heating phase, but developed a strong ion ITB followed by a disruption, as it is usually observed for stronger heating during current ramp-up. The reason for this different behaviour is an L-H transition (due to the reduced B_t) already in the current ramp-up phase, leading already in this phase to T_i values well above T_e. Such a target plasma is especially prone to develop an ion ITB with additional NBI heating. We refer to [11], in which the dilution of the thermal ions by the fast ion population produced by the NBI is identified as a key element to generate an ion ITB on ASDEX Upgrade due to stabilisation of ITG-modes.

3. Early versus late heating

Figure 5 also shows the equilibrated profiles for the late heating scheme and for lower q_{95}. As mentioned above, no reliable MSE data exist for most of the lower q_{95} discharges. Therefore we first focus on the q_{95}=4.8 case and will compare the MHD-modes and confinement of the lower q_{95} case further below. As can be seen from table 1 the early and late heating cases are most prominently separated by a 20 % higher H-factor (and stored energy) in the late heating case as well as by the q-profiles at the onset of the main heating. The differences of the equilibrated q-profiles at the end of the main heating are much smaller (figure 5) and an error analysis is required to decide whether these differences can be regarded as real. Figure 6 shows the q-profiles for both cases including local error-bars at the location of the MSE channels. These error bars overlap over the whole radius, but about half of the error bar is due to uncertainties of the exact shape of the flux surfaces. Since we are dealing with almost identical plasmas, the geometrical error must be largely correlated for both curves and should not be considered when deciding if the curves are different with respect to the error bars. With this argument we conclude that these two q-profiles are significantly different for $0.3 < \rho_{tor} < 0.6$. An additional difference is the MHD-behaviour: the early heating scheme triggers early (4,3)- or (3,2)-NTMs, whereas the late heating scheme shows only (1,1)-fishbones. We note here that both types of modes have been discussed in literature already to feedback on the current profile evolution. As mentioned above, (3,2)-NTMs in hybrid-discharges in DIII-D are discussed in [2]. For fishbones we refer here to publications on the early improved H-modes in ASDEX Upgrade which were dominated by fishbones [12], although early heating was applied. A significant difference to the recent early-heating scheme was the ramp-up in a limiter configuration. With this limiter ramp-up the T_e-profiles were significantly more peaked ($T_e(0)/T_e(0.8)$ is about a factor 2 larger) as compared to the diverted ramp-up used presently. This should lead to a higher current density and a lower q-value on axis, which may be the reason that (1,1)-fishbones appeared under these conditions instead of (4,3) or (3,2) NTMs. The confinement of these first fishbone-dominated improved H-modes is similar to the recent fishbone-dominated late-heating scheme. The different confinement properties of the H-modes obtained with the present early and late heating scheme

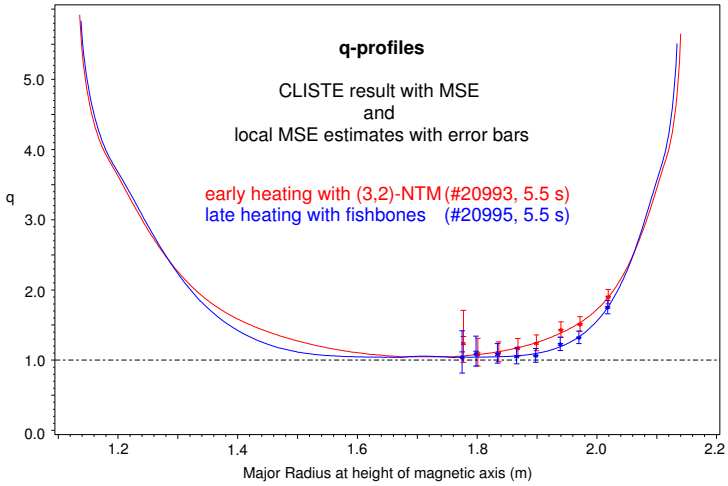

Figure 6: Local error bars of the q-profile from MSE-diagnostic for the early (red) and late (blue) heated discharges from fig. 2 towards the end of the heating phase at 5.5s. The profiles are identical to those shown with same colour and solid lines in fig. 5.

(fig. 2) may be a direct consequence of the different MHD-modes and the related differences in the current profile. As possible mechanisms one can either think of the direct influence of the NTM by short-cutting magnetic heat insulation across the island width or of effects of the modified current profile on core and/or pedestal transport. For the pair shown in figure 2 all three effects may play a role. Figure 7 shows temperature and density profiles of the respective discharges, fitted to ECE and Thomson scattering (TS) for T_e, CXRS for T_i and far-infrared interferometry plus Lithium-beam-diagnostic for n_e. We note that the temperature values close to the pedestal top are similar in both cases but the gradients in the confinement zone are larger for the late-heating case. The difference in the density is essentially due to a variation at the pedestal top. The common polynomial fit of the two T_e-diagnostics hides the fact that the ECE profiles are only different inside $\rho_{tor} \approx 0.5$ which is approximately the position of the NTMs in the early-heated discharge, whereas the CXRS and TS data rather show the wide variation also shown by the fits in figure 7. The ECE-data indicate a direct effect of the NTM, whereas the variation of the gradients over a wider radial range would require a different explanation.

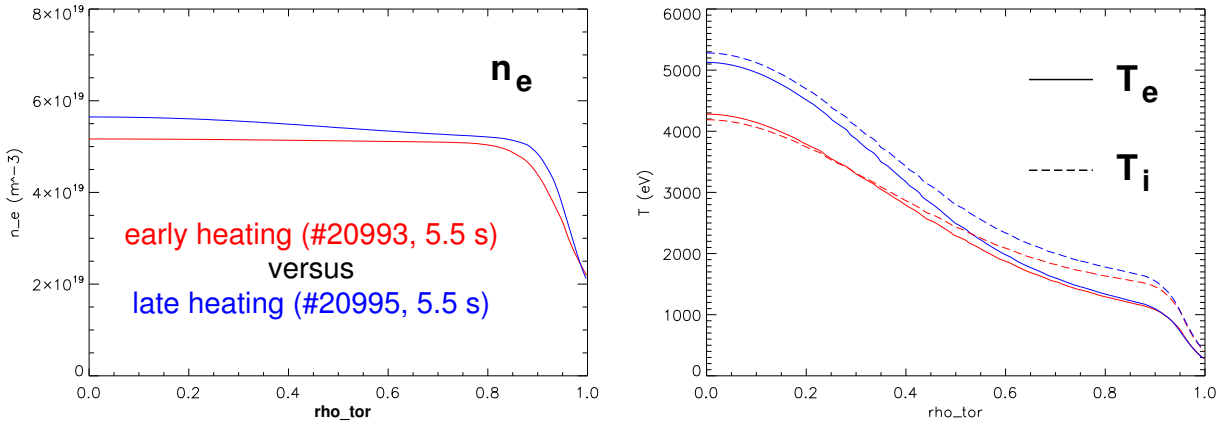

Figure 7: Electron density profiles and electron and ion temperature profiles for the early (red) and late (blue) heated discharges from figs. 2,6 (at 5.5 s).

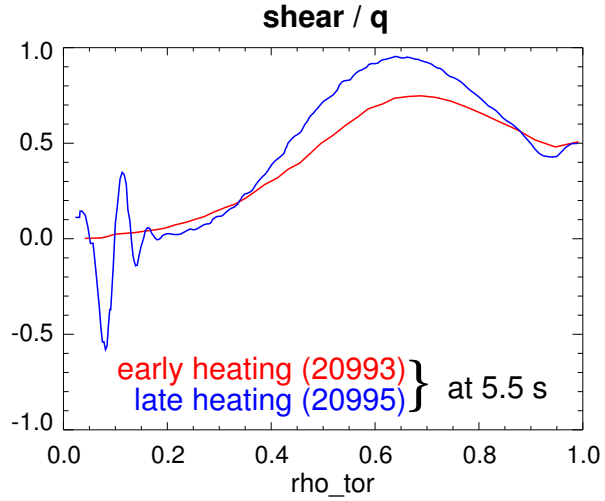

Figure 8: The inverse gradient length of q, s/q for the early (red) and late (blue) heated discharges also shown in figures 2,6,7. From figure 6 it is clear that the differences are only relevant in the range $0.3 < \rho_{tor} < 0.6$.

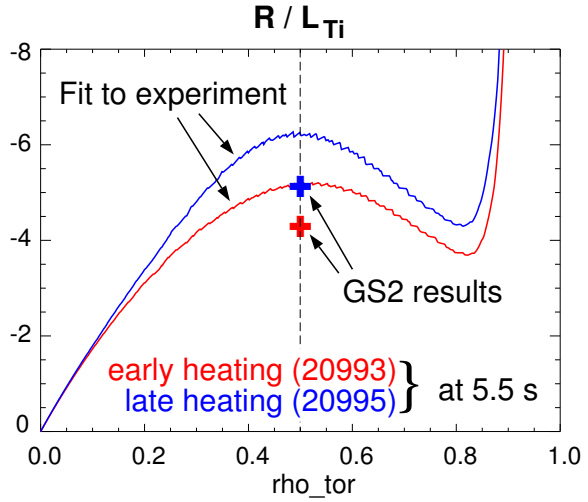

Figure 9: solid lines correspond to R/L_{Ti} calculated from the fits to the experimental T_i-profiles as shown in figure 7. Crosses correspond to critical values of R/L_{Ti} obtained for the onset of ITG turbulence by the linear gyro-kinetic GS2 code.

Since we have reliable q-profiles for these cases we calculate the ratio of magnetic shear and safety factor, i.e. s/q, known to influence the critical temperature gradient length for ITG turbulence. Figure 8 compares the profiles of s/q for both cases and the solid lines in figure 9 are the R/L_{Ti} profiles obtained from the fits to the experimental T_i data. In the same figure, the linear thresholds of R/L_{Ti} at mid-radius for the two plasmas are shown. These have been computed with GS2 [13] as the values of R/L_{Ti} at which the maximum growth rate is equal to the value of the $E \times B$ shearing rate $\omega_{E\times B}$ [14]. The calculations are made in such a way to quantify exclusively the effect due to the variation of the shear and safety factor profiles in the two plasmas. Comparing both discharges we note that the difference of the calculated threshold values is close to that of the measured values. This shows that the theoretically predicted effects on ion heat transport due to the observed changes in the current profile are large enough to cause changes of the T_i profiles which are in the observed range.
As mentioned above, also the pedestal pressure is higher in the late-heating case due to increased pedestal density. It is well known that the plasma current in the plasma edge has a strong influence on pedestal behaviour and therefore modifications of the current profile could in principle influence the pedestal. Unfortunately, we do not have good enough edge data for these discharges to reconstruct the bootstrap current in the edge region properly. Nevertheless, analysis of the plasma edge under these conditions is reported for a pair of discharges from the previous campaign in [15], showing that the width of the steep density-gradient zone is similar but steeper density gradients in the H-mode pedestal and a higher separatrix density lead to higher pedestal densities in the late-heating case. Unfortunately, these discharges with good edge measurements did not have proper MSE-data, such that also for this pair it is not possible to link central current profile and edge current profile.

4. Conclusions for current ramp-up

In the previous section it was described that the specific early heating scenario had poorer energy confinement most likely due to the NTMs or the related q-profile modifications. This correlation can occasionally be observed also in a single flattop phase during which the (4,3) or (3,2) NTM appears or disappears: In [16] a case is shown, for which the (3,2)-mode does set in well after the start of the main heating. Before, the main heating phase showed only a weak (5,4)-NTM. Immediately after the onset of the (3,2)-mode follows a reduction of the stored energy of more than 10%. Vice versa, the late-heated discharge at $q_{95} = 4.0$ (#20997) of our series comes up with a (4,3)-NTM and some seldom fishbones. As time evolves the fishbone bursts become longer and more frequent. Finally fishbones dominate and the NTM changes to (5,4) as shown in figure 10. The figure also shows the increase of the H-factor correlated with this change in MHD-behaviour. From this discharge it is clear that (3,2) or (4,3) NTMs are not necessary to reach high values of β (here $\beta_N = 2.8$, examples in [7] reach $\beta_N = 3.0$ with fishbones but no NTM). In terms of energy confinement it is even beneficial if these NTMs can be avoided. From the q-profile evolution shown in figure 4 it seems that in the early-heated discharges the NTM sets in as the q-profile drops to the corresponding q-values. As the central q-profile is very flat at that time point, the shear in the region around $q \approx 1.5$ is close to zero which facilitates the formation of an NTM. For the late heating the central current profile is already flat when the heating sets in and the central value is close to unity, favouring the occurrence of fishbones. In this case the shear at $q = 3/2$ is strong, possibly stabilising the mode, although β is higher. In terms of a start-up recipe these results suggest that for the onset of the main heating a flat central q-profile with $q \approx 1$ should be aimed at. In ASDEX Upgrade this was possible with an ohmic plasma ramped-up in a divertor configuration, but most likely also with early heating of a plasma ramped-up in a limiter configuration. There may be other ways, especially with dedicated tools such as LHCD [4] or ECCD to modify the current profile before the onset of the main

heating or during the main heating. Still the use of these tools may require subtle adjustments: DIII-D experiments on stabilisation of the (3,2)-mode with ECCD [2] resulted in larger sawteeth and no fishbones were reported. Seemingly, the q-profile on axis dropped well below unity, indicating that it may be necessary to counteract the full relaxation of the q-profile when stabilising the NTM. On ASDEX Upgrade it was possible to achieve sawtooth-free fishbone-dominated high β_N operation at $q_{95} \approx 3$ after stabilising a (3,2)-NTM [7]. As mentioned above, the NBI driven current may be important as well for the q-profile evolution, therefore it was kept constant in this study. Still it was different in the first fishbone-dominated improved H-modes in ASDEX Upgrade [1]. An extension of this study including variation of the beam sources is planned, although previous experiments showed that the q-profile is hardly modified by off-axis NBCD in strongly heated H-modes [17].

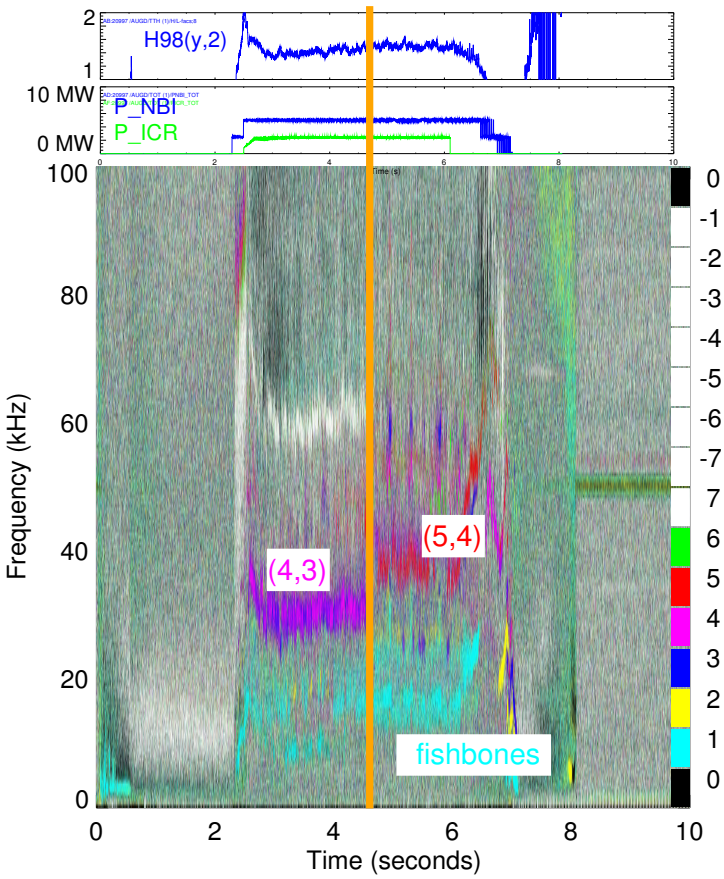

Figure 10: Late heating at $q_{95} = 4.0$ (#20997): time traces and MHD activity. From 2.5 to 4.5 s fishbone activity increases. Finally the NTM changes from (4,3) to (5,4).

References

[1] GRUBER, O. et al., Phys. Rev. Lett. **83** (1999) 1787.
[2] WADE, M. R. et al., Nucl. Fusion **45** (2005) 407.
[3] IDE, S. et al., Nucl. Fusion **45** (2005) S48.
[4] JOFFRIN, E. et al., Nucl. Fusion **45** (2005) 626.
[5] GRUBER, O. et al., Plasma Phys. Controlled Fusion **47** (2005) B135.
[6] ITER Physics Basis, Nucl. Fusion **39** (1999) 2137.
[7] SIPS, A. C. C. et al., in *this Conference*, pages EX/1–1, 2006.
[8] SUTTROP, W. et al., in *this Conference*, pages EX/8–5, 2006.
[9] MAGGI, C. F. et al., in *this Conference*, pages IT/P1–6, 2006.
[10] SIPS, A. C. C. et al., Plasma Phys. Controlled Fusion **44** (2002) B69.
[11] TARDINI, G. et al., in *Europhysics Conference Abstracts (CD-ROM, Proc. of the 32nd EPS Conference on Plasma Physics, Tarragona, 2005)*, volume 29C, pages P–2.028, Geneva, 2005, EPS.
[12] GÜNTER, S. et al., Nucl. Fusion **39** (1999) 1535.
[13] KOTSCHENREUTHER, M. et al., Comput. Phys. Commun. **88** (1995) 128.
[14] WALTZ, R. et al., Plasma Phys. **1** (1994) 2229.
[15] HORTON, L. D. et al., in *Europhysics Conference Abstracts (CD-ROM, Proc. of the 33th EPS Conference on Plasma Physics, Rome, 2006)*, pages P–2.140, Geneva, 2006, EPS.
[16] NA, Y.-S. et al., Nucl. Fusion **46** (2006) 232.
[17] GÜNTER, S. et al., in *Europhysics Conference Abstracts (CD-ROM, Proc. of the 32nd EPS Conference on Plasma Physics, Tarragona, 2005)*, volume 29C, pages P–4.075, Geneva, 2005, EPS.